EUROMET Project 822 'Comparison of Neutron Fluence Measurements for Neutron Energies of 15.5 MeV, 16 MeV, 17 MeV and 19 MeV' (EUROMET.RI(III)-S2)

Results of the Comparison

G. Lövestam[1], R. Nolte[2], N. Roberts[3]

[1] Institute for Reference Materials and Measurements (IRMM), Geel, Belgium
[2] Physikalisch-Technische Bundesanstalt (PTB), Braunschweig, Germany
[3] National Physical Laboratory (NPL), Teddington, United Kingdom

Abstract

Neutron reference fields in the energy range above 15 MeV are produced using the T(d,n)^{4}He reaction and solid-state Ti(T) targets. The potential presence of non-monoenergetic neutrons from parasitic (d,n) reactions induced in the target materials makes this energy range particularly challenging for reference instruments which cannot discriminate the neutron energy, such as long counters or activation foils. Therefore, a supplementary comparison was carried out in the energy range from 15.5 MeV to 19 MeV involving reference instruments of different sensitivities to non-monoenergetic neutrons. The spectral distributions of the neutron beams were characterized by time-of-flight measurements and by Monte Carlo simulations.

1. Introduction

The CCRI(III)-K10 key comparison on neutron fluence measurements in monoenergetic neutron fields [1] comprised energies up to 14 MeV. Most of the methods and procedures used in the comparison exercise can also be applied for the energy range from 14 MeV to 20 MeV. However, a few specific aspects need to be considered for these neutron fields which are produced using the T(d,n) reaction and Ti(T) solid state targets. Most of the (d,n) reaction channels for target impurities like carbon and oxygen, as well as for titanium and for backing material such as silver have positive *Q* values. The deuteron energies required for the production of neutron fields with energies up to 17 MeV are below 1.3 MeV. Although the cross sections should be rather low at these deuteron energies a small contribution of neutrons from reactions with impurities cannot be excluded. In addition, monoenergetic neutrons of lower energy are produced by the D(d,n) reaction with the deuterium impurity present in Ti(T) targets or implanted in the backing. Usually, the deuterium contamination amounts to about 1 % of the tritium content. The problem is much more severe for the 19 MeV neutron field which is produced by 2.55 MeV deuterons. Here it is well known that the fluence of continuum neutrons can amount to more than 50 % of the total fluence [2].

For the neutron energy range below 20 MeV the maximum energy of the non-monoenergetic neutrons is below 10 MeV. In principle, blank targets can be used to subtract experimentally the non-monoenergetic neutrons. This requires, however, that the blank Ti targets matches exactly with the Ti(T) target. In practice, this turns out to be difficult to achieve since at least the contamination with oxygen, carbon and deuterium as well as the amount and spatial location of implanted deuterium is usually different.

Recoil proton telescopes (RPT) usually have sufficient energy resolution to discriminate the fluence of non-monoenergetic neutrons from the fluence of monoenergetic neutrons since the energy of the non-monoenergetic neutrons is at least 5 MeV lower than that of the monoenergetic neutrons. Hence, an experimental determination of the non-monoenergetic neutron fluence is not necessary. This is different, however, if a long counter (LC) is used for

fluence measurements in the energy range from 15 MeV to 20 MeV because this instrument has virtually no energy discrimination capability. Therefore long counters were only used for neutron energies below 15 MeV until now. The same problem as for long counters arises also when activation foils are employed for fluence measurements, although the response to lower energy neutrons is much lower due to the threshold in the activation cross section.

Therefore the Institute for Reference Materials and Measurements (IRMM), the Physikalisch-Technische Bundesanstalt (PTB) and the National Physical Laboratory (NPL) initiated the EUROMET project 822 to compare their neutron fluence measurement capabilities in neutron fields with a non-monoenergetic spectral contribution. In this exercise, the IRMM and the PTB employed RPTs while the NPL used its de Pangher long counter and aluminium activation foils. Since the spectral distribution of the low-energy continuum depends on target properties, all participants had to carry out their measurements at the same facility and at the same measurement conditions. Therefore the same procedure as for the CCRI(III)-K10 comparison was chosen for the EUROMET project, which was registered in the Key Comparisons Data Base (KCDB) as the EUROMET.RI(III)-S2 comparison

The measurements with the recoil proton telescopes and the long counter were carried out in December 2004 in the low-scatter hall of the PTB accelerator facility. The nominal mean energy of the uncollided neutrons produced by the T(d,n) reaction were 15.5 MeV, 16.0 MeV, 17.0 MeV and 19.0 MeV. An additional measurement with the PTB RPT and the NPL aluminium activation foils was carried out in March 2005 at a neutron energy of 16.0 MeV. Table 1 summarizes the measurements carried out during the comparison.

Table 1. Overview of the measurements carried out during the EUROMET project 822. The deuteron energy and the nominal neutron energy are denoted by E_d and E_n, respectively. The energy loss in the Ti(T) layer is denoted by ΔE_d. All target parameters are nominal values.

date	E_n / MeV	E_d / keV	ΔE_d / keV	target acronym	participants
2004-12-06	16	778	332	AG-95-1	PTB, NPL(LC)
2004-12-07	17	1259	206	GU-80	IRMM, PTB, NPL(LC)
2004-12-08	19	2664	267	GU-75	IRMM, PTB, NPL(LC)
2004-12-09	15.5	621	386	AG-95-1	IRMM, PTB, NPL(LC)
2004-12-10	16	778	332	AG-95-1	IRMM, PTB
2005-04-20	16	778	332	AG-95-1	PTB, NPL(Act.)

The participants were asked to measure the fluence of the monoenergetic neutrons and to report the calibration factor $C = \Phi/M$ of one of the neutron monitor detectors. Here M denotes the corrected reading of the monitor and Φ the measured neutron fluence at 1 m distance from the Ti(T) target in vacuum.

This report describes the characterisation of the neutron fields, the instruments and procedures used by the participants. Frequent reference is made to the final report of the CCRI(III)-K10 comparison [1]. Some of the results of the neutron field characterisation and monitoring procedure were distributed to the participants earlier as a basis for their analysis. They are reproduced as appendices 2 and 3 of this report with minor, purely editorial, modifications.

2. Characterisation of the neutron fields and determination of the monitor readings

The accelerator settings and parameters of the targets used for producing the neutron fields are reproduced in Tab. 1 of appendix 2. All targets employed for the comparison had already been in use for several years. Hence, the tritium contents were significantly smaller than the T/Ti ratio of about 1.5 expected for fresh targets of high quality. The AG-95-1 target showed also a very inhomogeneous spatial distribution of the tritium loading. For the GU-75, target a blank Ti target with the same nominal thickness of the Ti layer was available. For the measurements in the 19 MeV neutron field, this blank target was used to subtract the contribution of neutrons resulting from (d,n) reactions with target impurities and backing material. It was, however, already known before these measurements that the GU75 target and the blank target did not match perfectly, in particular because of differences in the carbon and oxygen contamination.

The spectral distributions of the neutron fields were measured using a 2"×2" NE213 detector and the time-of-flight (TOF) technique. The results of the TOF measurements are reported in appendix 2. As outlined there, the measured fluence of non-monoenergetic neutrons always exceeded that resulting only from scattering of monoenergetic neutrons in the target assembly as calculated using the TARGET code [3]. The spectral fluence distributions used by the participants were a combination of experimental spectra below the matching energy E_{cont} and of TARGET calculations in the region of the monoenergetic peak above E_{cont}. The matching energy E_{cont} ranged from 11.7 MeV for the 15.5 MeV field to 15.8 MeV for the 19 MeV field. The contributions of neutrons from D(d,n) reactions with impurity deuterium were included in these spectral distributions.

The procedure used to determine the monitor readings was essentially the same as for the CCRI(III)-K10 comparison. The count rates for of two long counters positioned at 16° (NM) and 100° (PLC) were recorded together with the beam charge Q. In addition, the count rate of a ^{3}He counter covered by borated polyethylene was recorded. This detector was positioned close to the target at a backward angle. As discussed in detail in appendix 2, the count rate of the three neutron monitors were corrected for neutron inscattering form the reference instruments in the neutron field as well as for dead time losses.

For stable beam focusing conditions and homogeneous tritium loading, the beam charge Q should be strictly proportional to the neutron yield for a specific neutron energy. Indeed, the ratio of the corrected monitor readings to beam charge was found to vary by less than 1 % for most of the irradiations. Only for the measurements at 15.5 MeV and 19 MeV, a drift of the monitor ratios by several percent at the beginning of the measurements was observed. Since all three monitors were affected in the same way, these drifts can be attributed to changes in the beam focusing, possibly caused by warming-up effects.

The NM monitors have the highest sensitivity of the three neutron monitors. Therefore this monitor was selected to evaluate the requested calibration factor C.

3. Measurements carried out by the participants

3.1. IRMM

The IRMM employed its recoil proton telescope TC3 for the measurement. This instrument uses a combination of two proportional counters and a CsI(Tl) scintillation detector to detect recoil protons emitted from a polyethylene radiator with a surface mass density of 44.2 mg/cm^2. The neutron detection efficiency of the instrument is calculated according to Bame [4]from the geometrical data, the radiator properties and the n-p scattering cross section using a combination of analytical and numerical integration. The n-p cross

section data were taken from the analysis by Hopkins and Breit which is virtually identical with the ENDF/B-IV evaluation.

Due to problems with the second proportional counter, the usual threefold coincidence requirement could not be used to discriminate signals caused by recoil protons from backgrounds events in the CsI(Tl) detector. Instead, a second-order polynomial was fitted to the CsI(Tl) pulse-height spectra in the region outside the recoil proton peak and used to subtract the background in the peak region [5]. Measurements were carried out at several distances to the target. The results were corrected for neutron fluence attenuation in the aluminium entrance window and in the air between the target and the RPT, for the interaction of recoil protons with the wires of the proportional counters and for dead time losses. The final result specified is the mean value of the measurements at different distances. The dominating sources of uncertainty were the statistical uncertainty of the number of events in the region of the recoil proton peak, the uncertainty of the fitting procedure used for background subtraction and the uncertainty of the number of protons in the radiator.

3.2. PTB

The mechanical construction of the PTB recoil telescope RPT1 is very similar to that of the IRMM telescope but a 1.5 mm thick silicon surface barrier detector instead of a CsI(Tl) scintillation detector is used to detect the recoil protons. Also some of the geometrical parameters of the instruments are slightly different from those of the IRMM RPT. Because the thickness of this detector is insufficient to stop recoil protons with energies higher than 15 MeV aluminium degrader foils with thicknesses ranging from 0.285 mm to 0.625 mm were placed in front of the silicon detector to reduce the energy of the recoil protons. A threefold coincidence requirement was used to discriminate recoil protons originating from a tristearin radiator with an areal mass of 10.085 mg/cm^2 from background events.

The neutron detection efficiency of the instrument was calculated according to the procedure described by Bame *et al*. [4]. Total n-p scattering cross sections were taken from the ENDF/B-IV evaluation. The angular distribution was very similar to that given in ENDF/B-IV with a maximum deviation of 0.15 % at a centre-of-mass scattering angle of 180°. Measurements were carried out at a single distance for each neutron energy. The measurement results were corrected for neutron fluence attenuation in the aluminium entrance window and in the air between the target and the RPT and for dead time losses. A correction was also applied for the contribution of the low-energy tail of the pulse-height spectra to the number of events detected in the peak region. The dominating sources of uncertainty were the statistical uncertainty of the number of events in the region of the recoil proton peak and the uncertainty of the number of protons in the radiator.

As outlined in Appendix 2, there is evidence for a neutron component in the 17 MeV field resulting from T(d,n)^{4}He reactions with tritium diffused into the backing. The fluence of this component is about 4.3 % of the peak fluence and the mean energy is about 15 MeV. This possible presence of this component was accounted for by using a weighted average of the n-p cross sections for 15 MeV and 17 MeV. This effective cross section was 0.5 % higher than the cross section for monoenergetic 17 MeV neutrons.

3.3. NPL

The NPL used its de Pangher LC for fluence measurements at all four neutron energies. The efficiencies and the effective centres of the LC were calculated using the MCNP Monte Carlo code and verified by measurements using radionuclide neutron sources. The emission rates of these sources were determined using the NPL manganese bath. Measurements were performed at several distances from the target for each neutron energy. Two dedicated shadow cones were used to determine the contribution of room-return neutrons to the number

of events registered with the LC. The results were corrected for the contribution of non-monoenergetic neutrons as determined by PTB using the TOF method and calculations with the TARGET code. The corrections ranged from 7 % for 17 MeV field to 30 % for the 19 MeV field. Additional corrections for dead time losses and fluence attenuation in air were applied.

For the activation measurements at 16 MeV, two Al foils 0.3 mm and 0.14 mm in thickness were activated in a back-to-back geometry at a distance of 92 mm from the target using a low-mass sample holder. The foils were irradiated for about 4.6×10^4 s and then transported to the NPL where β-counting started about 17 h after the end of the irradiation. The β-counting efficiency of the NPL foils had been determined earlier using the $4\pi\,\beta\gamma$ coincidence technique. The measurement result was determined from the measured activity using the foil mass and spectrum-averaged cross sections for the $^{27}Al(n,\alpha)^{24}Na$ reaction which were calculated from the point cross sections of the ENDF/B-VI evaluation as well as those published by Wagner *et al*. [6]. Corrections for variations of the neutron fluence during irradiation and for decay between the end of the irradiation and start of the activity measurement were applied. The final result reported by the NPL is the mean of the results obtained using the two cross section data sets. The relative deviation of the two results from the mean was ±0.0085.

4. Results

4.1. General remarks

Since the present exercise is organized as a supplementary comparison, the participants reported different results for each method used. It was also not required to calculate a key comparison reference value (KCRV) and degrees of equivalence (DOE). Instead, the results of the participants were compared with the weighted mean of all stated results. Generally, the analysis followed the procedure outlined in [6]. It should, however, be noted that at least the results stated by IRMM and PTB are expected to be correlated to a considerable extent as the same kind of reference instrument and very similar cross section data sets were used. The main difference between the PTB and IRMM measurements is the method used to determine the number of recoil protons produced by uncollided monoenergetic neutrons.

4.2. Evaluation of the results

At 16 MeV two measurements were carried out by PTB using their RPT1 telescope. The first measurement, PTB-1, was carried out in connection with the NPL measurement on 2004-12-06 while the second measurements PTB-2 was performed in connection with the IRMM measurement on 2004-12-10. A third measurement PTB-3 was carried out together with the activation of the NPL aluminium foils on 2005-04-20.

As for the CCRI(III)-K10 comparison, the weighted mean of the PTB results for the 16 MeV fields was calculated using only the uncorrelated components of the uncertainties as weighting factors. The correlated component of the relative uncertainties was added quadratically to the uncertainty of the weighted mean. This measurement result was used together with the results of IRMM and NPL to derive the weighted mean of all results. This procedure ensured that repeated measurements with the same instrument did not introduce a significant bias towards one participant. Table 2 and Fig. 1 summarise the results of the repeated measurements carried out with the PTB telescope at 16 MeV. The good agreement of the data shows the reproducibility of the neutron field despite the inhomogeneity of the tritium loading observed during the comparison (cf. Appendix 1).

Table 2. Results obtained with the PTB telescope for the 16 MeV neutron field. The calibration factor and its absolute and relative standard measurement uncertainties are denoted C, u_C and u_{rel}, respectively. The uncorrelated and correlated contributions to the relative uncertainties are denoted $u_{rel,non}$ and $u_{rel,cor}$, respectively. The weighted mean was calculated using $u_{rel,non}$ as weights. A correlated component of 0.026 was added quadratically to the relative uncertainty of the weighted mean to yield the total uncertainty for the mean result.

date	acronym	C / cm^{-2}	u_C / cm^{-2}	u_{rel}	$u_{rel,non}$	$u_{rel,cor}$
2004-12-06	PTB-1	2.255	0.070	0.031	0.018	0.026
2004-12-10	PTB-2	2.196	0.067	0.031	0.017	0.026
2005-04-20	PTB-3	2.257	0.076	0.034	0.022	0.026
	weighted mean	2.231	0.062	0.028		

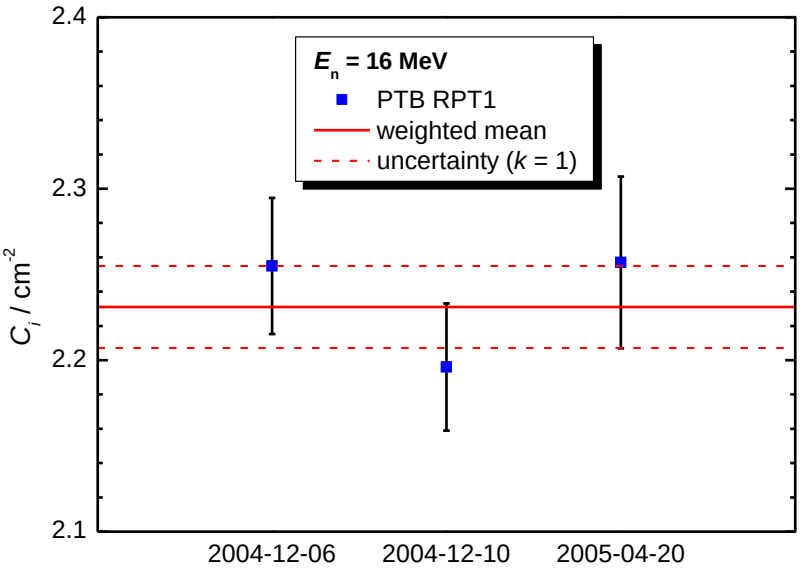

Fig. 1. Calibration factor C for the 16 MeV field measured using the PTB telescope RPT1 at different dates. The error bars show the uncorrelated component of the total uncertainty only. The weighted mean and its uncertainty (k = 1) are indicated by the solid and dashed lines.

The calibration factors C as measured by the participants are displayed in Fig. 2a. The weighted mean $\overline{C}$ and its standard measurement uncertainty $u_{\overline{C}}$ (k = 1) of all data reported is indicated as well. Fig. 2b shows the relative deviations $C/\overline{C} - 1$ from the weighted means. The numerical results are given in Appendix 1.

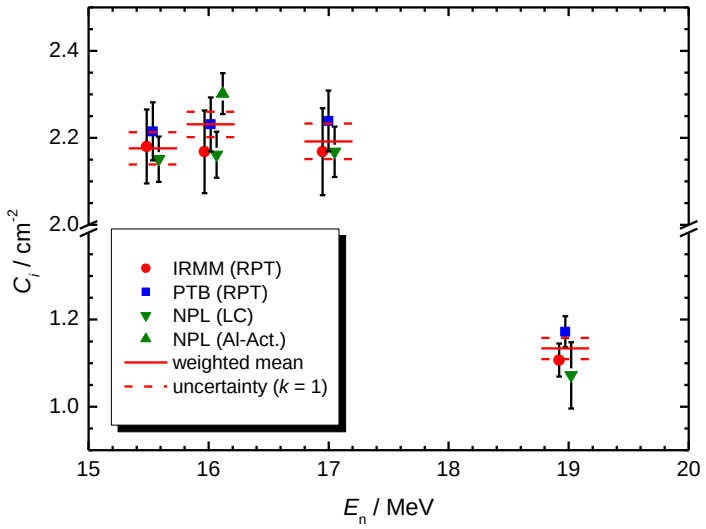

Fig. 2a. Calibration factor $C = \Phi/M$ of the 16° long counter monitor for the fluence Φ at a distance of 1 m from the Ti(T) target, corrected for fluence attenuation in air. The PTB result for the 16 MeV field is the weighted mean of all measurements carried during the entire comparison exercise (cf. Table 1). The NPL results for the activation measurement at 16 MeV was obtained using the ENDF/B-VI cross section data. The weighted mean of the results reported by the participants and its uncertainty are shown by the solid and dashed lines, respectively.

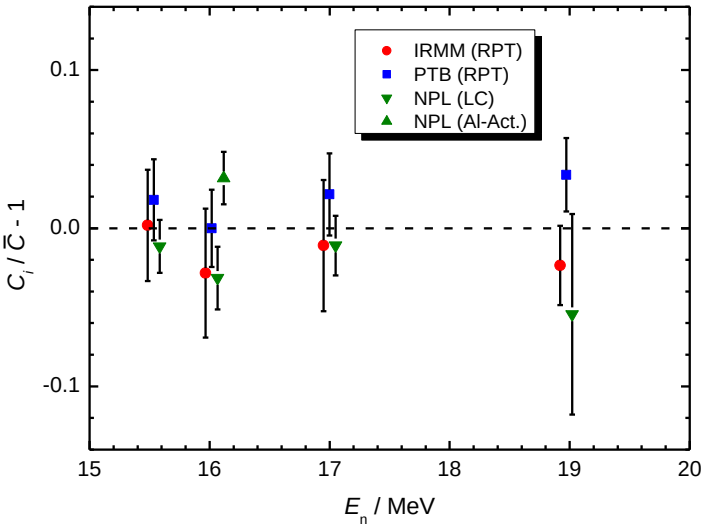

Fig. 2b. Relative deviation of the calibration factors C from the weighted means.

5. Discussion

As reported in Table 3 of Appendix 2, the relative contribution of non-monoenergetic neutrons, as measured using the NE213 detector, ranged between 4 % for 15.5 MeV and 25 % for 19 MeV. Despite these significant non-monoenergetic contributions, the results reported by the participants are consistent as indicated in Fig. 2b, where only two of the data points for the relative deviation from the weighted mean show a small but significant deviation from zero. This demonstrates that the uncertainty budgets specified by the participants are realistic. The results also show that the energy discrimination properties of the proton recoil telescopes

and the correction procedures used for the long counter and the activation foils are suitable for not perfectly monoenergetic neutron fields.

The remarkable agreement of the recoil telescope and the long counter is largely due to the very detailed and sophisticated modelling of the latter instrument using MCNP and the comprehensive set of measurements using radionuclide sources which are directly traceable to the activity standard with typical uncertainties of about 1 %. Together with the small type-A component for counting statistics, this explains why the smallest uncertainties were reported for the long counter, except for the 19 MeV case with its large correction for non-monoenergetic neutrons.

Despite the good overall agreement, there are two small but distinctive systematic trends to be observed in the results. For all energies, the PTB result is about 2 % higher than the results reported by IRMM for a very similar recoil proton telescope. To identify possible inconsistencies in the detection efficiencies, the PRTelescope code [8] developed for the IRMM telescope was used to calculate the efficiency of the PTB telescope for the neutron fields of the present comparison. The efficiencies were found to agree to better 0.5 % with the efficiency data used at PTB. As shown in the uncertainty budgets reported by IRMM and PTB, the nominal uncertainties given for the hydrogen content of the radiators also do not explain the observed trend. It is interesting to note that the deviation observed between the two telescopes is opposite to the results of the CCRI(III)-K10 comparison at 5 MeV and 14.8 MeV where the IRMM result was larger by about 2 % than the PTB result. A possible reason for the present observation could be the different procedures used by IRMM in the two comparisons for the determination of the number of detected recoil protons.

For all neutron fields up to 17 MeV, the NPL long counter yielded results which are also lower by about 2 % compared with the PTB proton recoil telescope. Also for the 19 MeV field the long counter result is smaller than the other results. If the corrections f_s applied for contribution of non-monoenergetic neutrons were too large due to an overestimation of the non-monoenergetic contribution (cf. Appendix 2), the resulting calibration factors C would also be too large. To investigate the consequence of this assumption, the NPL data for the neutron fields were rescaled in the following way:

$$C' = \left(1 - f_s \cdot \frac{\left(\Phi_{\mathrm{cont}} / \Phi_{\mathrm{peak}} \right)_{\mathrm{TARGET}}}{\left(\Phi_{\mathrm{cont}} / \Phi_{\mathrm{peak}} \right)_{\mathrm{exp.}}} \right) \cdot \frac{C}{(1 - f_s)} . \qquad (1)$$

This correction is only strictly valid if the response of the NPL long counter is independent of the neutron energy. The relative contributions of non-monoenergetic neutrons as measured with a scintillation detector and calculated using the TARGET code were taken from Table 3 of Appendix 2. The f_s values reported by NPL for distances of 2 m or 2.5 m from the Ti(T) target were employed. Fig. 3 shows the rescaled NPL data for the neutron energies below 19 MeV together with the PTB and IRMM results. The mean values are the same as in Fig. 2a.

The rescaled results are significantly above the RPT results and the deviation increases with neutron energy which is to be expected since the contribution from (d,n) reactions with titanium and silver should also increase with deuteron energy. This demonstrates that there is a background of non-monoenergetic neutrons in the investigated neutron fields in addition to the contribution resulting from target scattering of the monoenergetic neutrons as calculated by TARGET.

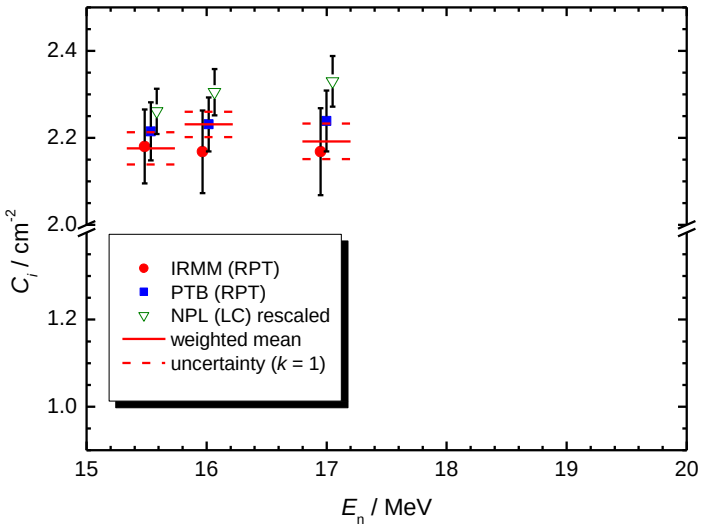

Fig. 3. Rescaled results of the NPL long counter measurements according to eq. (1). The RPT results and the mean values are the same as in Fig. 2a.

6. Conclusions

The present comparison showed that the measurement capabilities of the participants also yield consistent results for neutron fields above 14.8 MeV which are not strictly monoenergetic. This result is remarkable because instruments with and without sensitivity to non-monoenergetic neutrons of lower energy were employed. Hence, this comparison also confirms the procedures used to characterise the spectral distributions of the neutron fields.

References

[1] J. Chen et al., 'International key comparison of neutron fluence measurements in mono-energetic neutron fields – CCRI(III)-K10', Metrologia **44** (2007), Technical Supplement, 06005, www.bipm.org/utils/common/pdf/final_reports/RI/CCRI(III)/CCRI(III)-K10.pdf

[2] R. Böttger et al., 'Problems associated with the production of monoenergetic neutrons', Nucl. Instr. and Meth. **A282** (1989) 358-367

[3] D. Schlegel, 'TARGET user's manual', Laboratory report PTB-6.42-05-02, Physikalisch-Technische Bundesanstalt Braunschweig (2005)

[4] S.J. Bame et al., 'Absolute determination of monoenergetic neutron flux in the eenrgy range 1 to 30 MeV', Rev. Sci. Instr. **28** (1957) 997-1006

[5] G. Lövestam et al., 'The recoil proton telescope in non-coincidence mode for neutron fluence measurements', Nucl. Instr. and Meth. in Phys. Res. A, **566** (2006) 609–614.

[6] M. Wagner, H. Vonach, A. Pavlik et al., Physics Data 13-5, Fachinformationszentrum Karlsruhe 1990

[7] G. Ratel, 'Evaluation of the uncertainty of the degree of equivalence', Metrologia **42** (2005) 140-144

[8] G. Lövestam, 'PRTelescope ver. 29.04.2003'

Appendices

Appendix 1:

Numerical results reported by the participants

The participants reported the calibration coefficients $C = \Phi/M$ of the 16° long counter monitor. Here Φ and M denote the fluence in 1 m distance from the Ti(T) target, corrected for fluence attenuation in air, and the monitor reading corrected for inscattering and dead-time losses, respectively. The weighted means $\overline{C}$ were calculated using the uncertainties u_C as specified by the participants. For the 16 MeV neutron field, the weighted mean of all PTB results is indicated. The deviation of the results reported by the participants from the weighted mean and its uncertainty are denoted by D and u_D, respectively. The NPL result for the activation foil measurement is the mean of the results obtained using the cross section datasets of ENDF/B-VI and Wagner *et al*.. The reduced χ^2 is denoted by χ^2/ν.

15.5 MeV					
	C / cm^{-2}	u_C / cm^{-2}	u_C/C	D / cm^{-2}	u_D / cm^{-2}
IRMM	2.180	0.085	0.039	0.004	0.077
PTB	2.215	0.067	0.030	0.039	0.056
NPL(LC)	2.151	0.052	0.024	-0.025	0.037
$\overline{C}$	2.176	0.037	0.017		
χ^2/ν	0.29				

16 MeV					
	C / cm^{-2}	u_C / cm^{-2}	u_C/C	D / cm^{-2}	u_D / cm^{-2}
IRMM	2.168	0.095	0.044	-0.056	0.091
PTB	2.231	0.062	0.028	0.007	0.055
NPL(LC)	2.161	0.053	0.025	-0.063	0.044
NPL(Al-Act.)	2.302	0.047	0.020	0.071	0.037
$\overline{C}$	2.231	0.029	0.013		
χ^2/ν	1.49				

17 MeV					
	C / cm^{-2}	u_C / cm^{-2}	u_C/C	D / cm^{-2}	u_D / cm^{-2}
IRMM PTB NPL(LC)	2.168 2.239 2.168	0.100 0.070 0.058	0.046 0.031 0.027	-0.024 0.047 -0.024	0.091 0.057 0.041
$\overline{C}$ χ^2/ν	2.192 0.34	0.041	0.019		

19 MeV					
	C / cm^{-2}	u_C / cm^{-2}	u_C/C	D / cm^{-2}	u_D / cm^{-2}
IRMM PTB NPL(LC)	1.107 1.172 1.072	0.038 0.036 0.076	0.034 0.031 0.071	-0.027 0.038 -0.062	0.028 0.026 0.072
$\overline{C}$ χ^2/ν	1.134 1.15	0.025	0.022		

Uncertainty budget reported by the IRMM

Uncertainty budget

	Type	Relative standard uncertainty (k = 1) in percent					
		E_n = 15.535 MeV			E_n = 16.017 MeV		
	[8]	250	300	350	200	250	300
Calculation of efficiency							
a) Hydrogen content of radiator	B	1.00	1.00	1.00	1.00	1.00	1.00
b) Distance target to RPT and angle of RPT	B	0.12	0.12	0.10	0.14	0.12	0.12
c) Internal RPT geometry, including scattering by aperture and proportional wires	B	1.30	1.30	1.30	1.30	1.30	1.30
d) Total H(n,p)n cross section	B	1.00	1.00	1.00	1.00	1.00	1.00
e) Numerical solution of integrals	B	-	-	-	-	-	-
Analysis of measurements							
f) Number of events in peak of measured distribution	A	1.89	2.55	2.79	1.47	1.73	2.13
g) NM monitor normalisation	A	0.28	0.36	0.36	0.38	0.37	0.38
h) Spectrum fittings	B	1.88	2.74	2.56	2.74	3.42	4.28
i) Dead time and pile up effects	B	< 0.1	< 0.1	< 0.1	< 0.1	< 0.1	< 0.1
j) In/out scattering of neutrons to RPT	B	-	-	-	-	-	-
Combined relative uncertainty		3.30	4.23	4.27	3.68	4.30	5.17
Uncertainty for mean value		**3.9**			**4.4**		

Uncertainty budget, continued

	Type	Relative standard uncertainty (k = 1) in percent			
		E_n = 16.999 MeV			E_n = 18.971 MeV
	[8]	200	250	300	250
Calculation of efficiency					
a) Hydrogen content of radiator	B	1.00	1.00	1.00	1.00
b) Distance target to RPT and angle of RPT	B	0.14	0.12	0.12	0.12
c) Internal RPT geometry, including scattering by aperture and proportional wires	B	1.30	1.30	1.30	1.30
d) Total H(n,p)n cross section	B	1.00	1.00	1.00	1.00
e) Numerical solution of integrals	B	-	-	-	-
Analysis of measurements					
f) Number of events in peak of measured distribution	A	2.24	2.89	3.00	1.60
g) NM monitor normalisation	A	0.57	0.56	0.56	0.37
h) Spectrum fitting	B	3.02	3.22	3.31	2.21
i) Dead time and pile up effects	B	< 0.1	< 0.1	< 0.1	< 0.1
j) In/out scattering of neutrons to RPT	B	-	-	-	-
Combined relative uncertainty		4.26	4.77	4.90	3.36
Uncertainty for mean value		**4.6**			**3.4**

Uncertainty budget reported by the PTB

Reduced uncertainty budget for the neutron fluence measurements using the PTB recoil proton telescope RPT1.

	Relative standard uncertainty (k = 1) in percent				
	15 MeV	**16 MeV 22.64 cm**	**16 MeV 37.64 cm**	**17 MeV**	**19 MeV**
(n,p) cross section	1.00	1.00	1.00	1.10	1.00
Number of hydrogen atoms	0.50	0.50	0.50	0.50	0.50
Statistics of net counts	1.49	1.55	2.16	1.56	1.66
Source-detector distance	0.10	0.10	0.06	0.10	0.10
Lower integration boundary	0.58	0.58	0.58	0.58	0.58
Calculated efficiency factor	2.20	2.20	2.20	2.20	2.20
Attenuation correction for Al window and Ta backing	0.28	0.28	0.28	0.28	0.28
Attenuation correction for ambient air	0.03	0.03	0.03	0.03	0.03
Monitor uncertainty	0.64	0.84	0.50	0.84	0.32
Combined relative standard measurement uncertainty	**3.02**	**3.10**	**3.10**	**3.14**	**3.14**

Uncertainty budget reported by the NPL for the long counter measurements

Component uncertainties at 15.5, 16, 17, and 19 MeV

Input parameters	Neutron energy			
	15.5 MeV	16 MeV	17 MeV	19 MeV
Statistics & dead time	0.2 %	0.2 %	0.2 %	0.5 %
Scatter correction	0.3 %	0.3 %	0.4 %	0.3 %
Blank target correction	-	-	-	2.7%
De Pangher stability	0.4 %	0.4 %	0.4 %	0.4 %
M*	0.6 %	0.5 %	0.6 %	2.7 %
f_s	10 %	10 %	10 %	10 %
Σ_A	10 %	10 %	10 %	10 %
l	0.2 cm	0.2 cm	0.2 cm	0.2 cm
r	0.6 cm	0.6 cm	0.6 cm	0.6 cm
ε	2 %	2 %	2 %	2 %
NM statistics	0.2 %	0.3 %	0.3 %	0.2 %
NM stability	0.5 %	0.15 %	0.08 %	0.6 %
Total	2.4 %	2.5 %	2.6 %	7.1 %

* The uncertainty for M is the quadratic sum of the three or four components above

The above uncertainties correspond to the measurement at the target to long counter distance which gave the lowest uncertainty. For 15.5 MeV this was 200 cm, for 16 MeV it was 200 cm, for 17 MeV it was 250 cm, and for 19 MeV it was 200 cm.

Uncertainty budget reported by the NPL for the activation foil measurements

Component uncertainties for aluminium foil activation measurement at 16 MeV

Symbol	Source of uncertainty	Value (%)	Probability distribution	Divisor	u_i (%)
	Counting statistics	0.1	normal	1	0.1
F_T	Flux variations	0.005	normal	1	0.005
$\varepsilon_ß$	ß-counting efficiency	0.2	normal	1	0.2
K	K-correction	0.2	normal	1	0.2
$\sigma(E)$	Activation cross section (ENDF/B-VI, Wagner et al)	1.6	normal	1	1.6
E_n	Mean neutron energy (70 keV)	1.4	rectangular	$\sqrt{3}$	0.81
m	Foil mass	0.1	rectangular	$\sqrt{3}$	0.06
λ	Decay constant	0.1	normal	1	0.1
	Dead time correction	0.2	rectangular	$\sqrt{3}$	0.12
	Target – foil distance (0.7 mm)	1.5	rectangular	$\sqrt{3}$	0.89
f_s	Target scatter factor (10 %)	0.24	normal	1	0.24
$u(\varphi)$	Combined uncertainty	---	normal	---	2.03

Appendix 2:

EUROMET Project 822 'Comparison of Neutron Fluence Measurements for Neutron Energies of 15.5 MeV, 16 MeV, 17 MeV and 19 MeV'

Determination of the spectral fluences

Introduction

The EUROMET project 822 aims at the comparison of neutron fluence measurements for neutron energies above 14.8 MeV which were not covered in previous comparison exercises. The neutron fields were produced at the PTB low-scatter facility using the T(d,n) reaction with Ti(T) targets and deuteron beams with energies from 635 keV to 2664 keV. At these bombarding energies, production of background neutrons by (d,n) reactions with the Ti of the Ti(T) targets with the backing materials and with the deuterium contamination present in the Ti(T) layer has to be expected since many of the reaction channels are energetically possible. Measurements were carried out from 2004-12-04 until 2004-12-10 using recoil proton telescopes (IRMM, PTB) and a long counter (NPL). In addition, NPL used a liquid scintillation detector for supplementary measurements. At 2005-04-20, a comparison of a fluence measurement using the Al-foil activation technique with the PTB recoil proton telescope was carried out at a neutron energy of 16 MeV.

The recoil telescopes allow to separate the monoenergetic neutrons reaching the detector without further interaction (uncollided neutrons) from most of the neutrons scattered in the target assembly (collided neutrons) and from background neutrons. In contrast, the long counter has an almost constant sensitivity for all neutrons reaching the sensitive area. Therefore the measurements made with the long counter have to be corrected for the contribution of the collided and background neutrons. Even for the analysis of the recoil telescope measurement, the spectral distribution of the uncollided neutrons has to be available for the calculation of the mean energy.

Therefore time-of-flight (TOF) measurements were carried out separately to determine experimentally the spectral fluence of the background neutrons. The spectral fluence of the uncollided and collided neutrons were calculated using the TARGET code [1].

Target and deuteron beam parameters

The relevant target and deuteron beam parameters used for the comparison are listed in Table 1.

Table 1 Target and beam parameters used for the comparison. The deuteron energy and the nominal neutron energy are denoted by E_d and E_n, respectively. The surface mass densityof the Ti layer is denoted by m''_{Ti} and the number of T nuclei per Ti nucleus by n_T/n_{Ti}. The energy loss in the Ti(T) layer is denoted by ΔE_d. All target parameters are nominal values.

date	E_n / MeV	target acronym	m''_{Ti} / mg cm^{-2}	n_T/n_{Ti}	backing	E_d / keV	ΔE_d / keV
2004-12-06	16	AG-95-1	1.04	1.07	0.5 mm Ag	778	332
2004-12-07	17	GU-80	0.937	1.08	0.5 mm Ag	1259	206
2004-12-08	19	GU-75	1.904	0.94	0.5 mm Ag	2664	267
2004-12-09	15.5	AG-95-1	1.04	0.77	0.5 mm Ag	621	386
2004-12-10	16	AG-95-1	1.04	0.82	0.5 mm Ag	778	332
2005-04-20	16	AG-95-1	1.04	0.97	0.5 mm Ag	778	332

The homogeneity of the Ti(T) layers was inspected by measuering the count rate of the long counter monitor mounted at a neutron emission angle of 16° as a function of the azimuth angle Θ of the rotating target assembly. The spectra shown in Fig. 1 exhibit pronounced dips in the AG-95-1 target. These dips can be either due to a local depletion of Ti in the otherwise homogeneous Ti layer or to an inhomogeneous Ti(T) layer. In the first case, the spectral distribution of the neutrons produced by the T(d,n) reaction would not be much affected. In the second case, however, the variation in the deuteron energy loss would also affect the neutron spectrum.

Since the TOF measurement were carried out separately, i.e. after remounting the target assembly, the results of this measurement are not fully sufficient to assess the consequences of the target inhomogenity during the comparison measurements. The pilot laboratory was aware of this problem before the measurements and informed the participants accordingly. It regrets that no better suited targets were available at the time of the comparison.

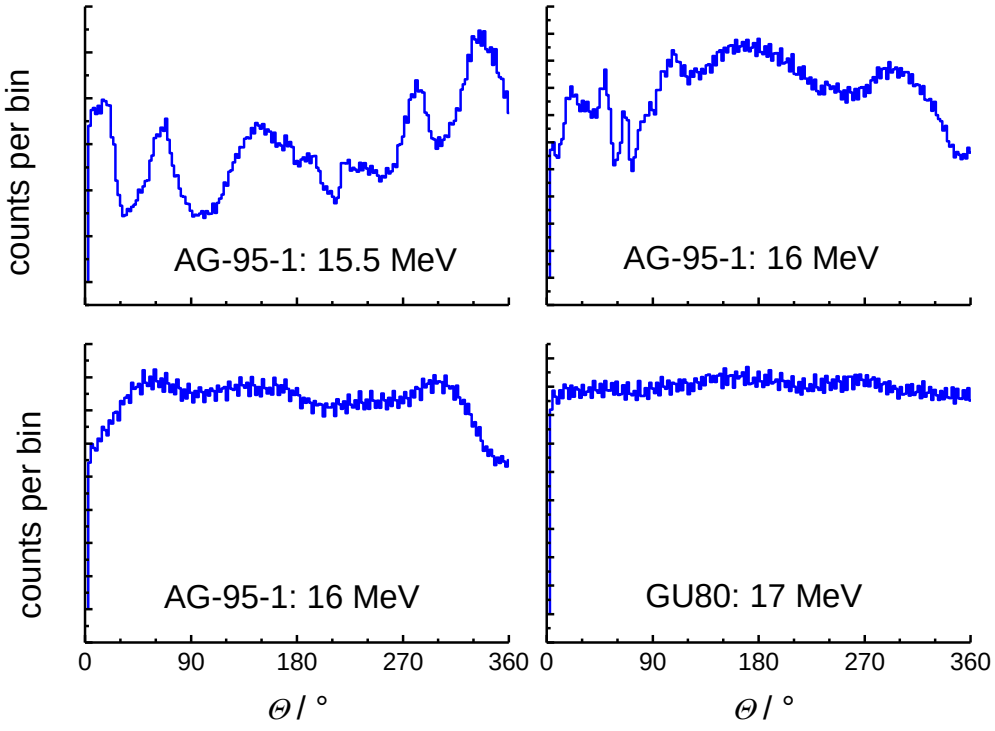

Fig. 1 Count rate of the long counter monitor positioned at a neutron emission angle of 16° as a function of the azimuth angle Θ of the rotating target assembly. The 16 MeV data sets in the upper and lower row were measured during the comparison of the active instruments and the Al foil activation, respectively.

Results of the TOF measurements

The TOF measurements were carried out from 2005-04-05 until 2005-04-08 using pulsed deuteron beams and a gain-stabilised 2″×2″ BC501 liquid scintillation detector. The centre of the detector cell was positioned at a distance of (6.277 ± 0.002) m from the Ti(T) target. The calibration of the TOF measurement was checked using a ORTEC 462 time calibrator. The total relative uncertainty (k = 1) of the TOF calibration was 1.5×10^{-3}.

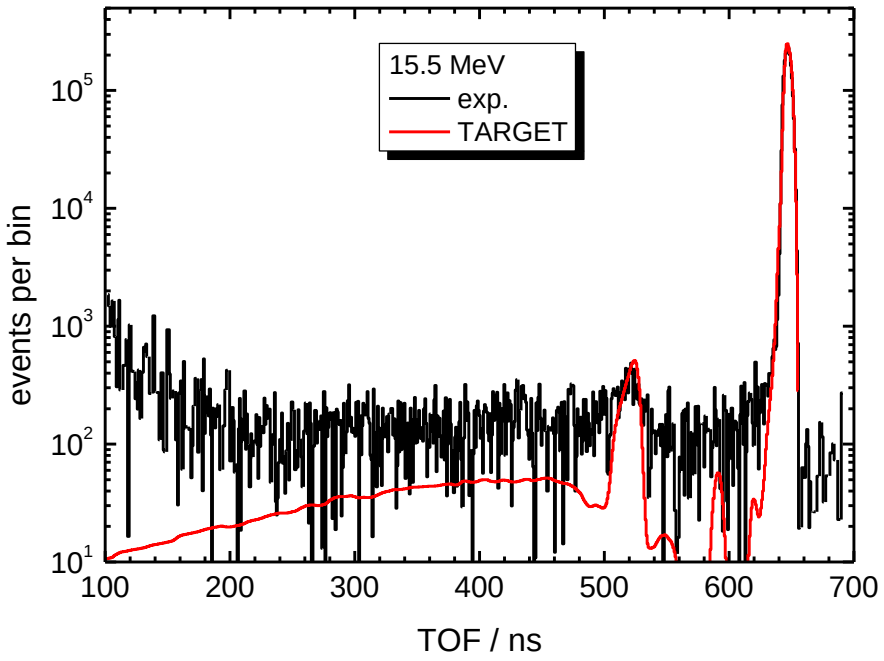

Fig. 2a TOF spectrum measured with the AG-95-1 target for 621 keV deuterons (black histogram) and calculated with TARGET (red solid line). The TOF parameter is related to the neutron and photon flight time t_n and t_γ: TOF = t_γ-t_n+TOF$_0$. HereTOF$_0$ is an arbitrary offset.

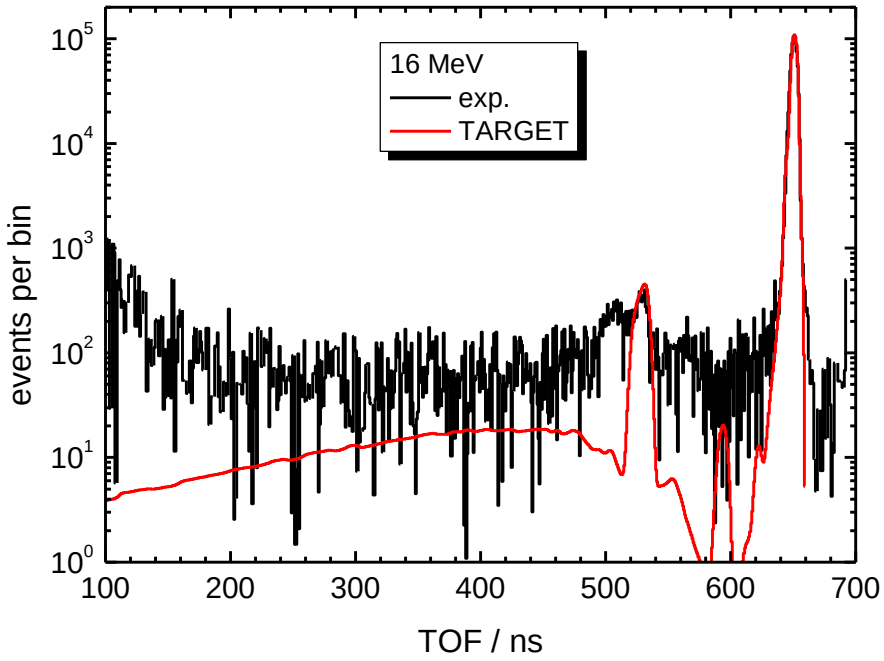

Fig. 2b TOF spectrum measured with the AG-95-1 target for 778 keV deuterons (black histogram) and calculated with TARGET (red solid line)

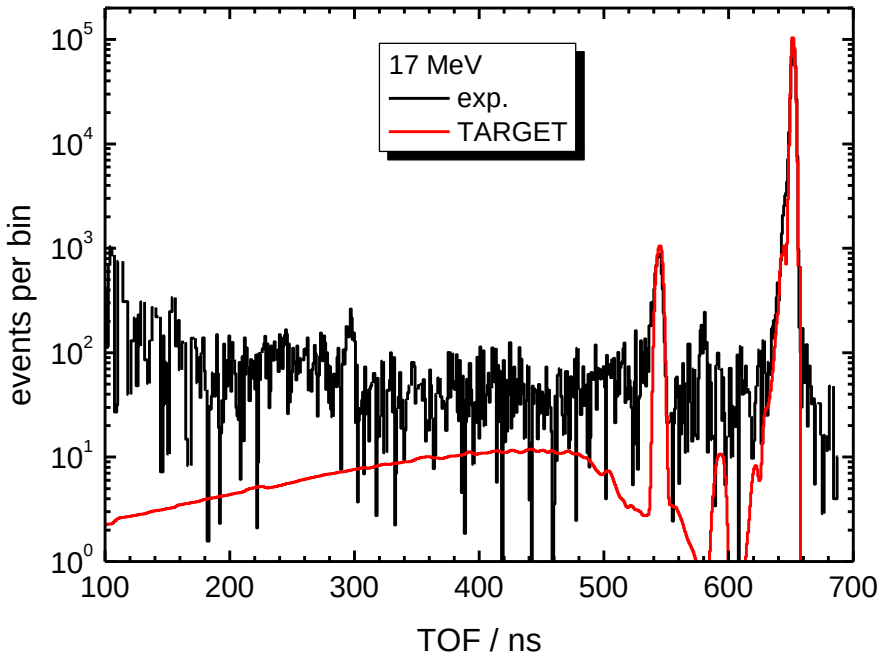

Fig. 2c TOF spectrum measured with the GU80 target for 1259 keV deuterons (black histogram) and calculated with TARGET (red solid line).

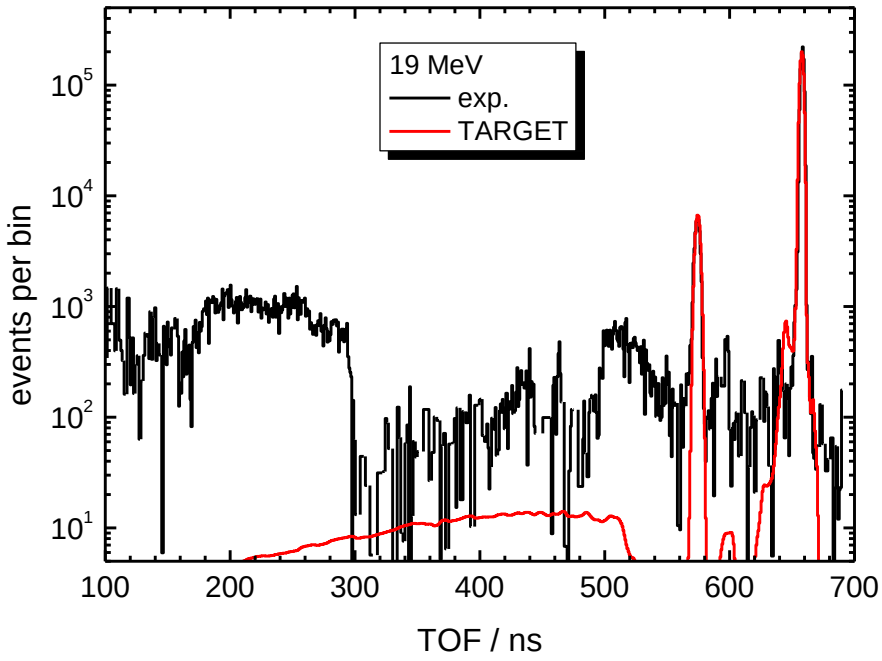

Fig. 2d TOF spectrum measured with the GU75 target for 2664 keV deuterons (black histogram) and calculated with TARGET (red solid line). The blank target measurement was subtracted from the experimental spectrum.

The detection thresholds of the low-gain (LG) and high-gain (HG) pulse-height branches were set to the pulse height produced by 250 keV and 60 keV electrons, respectively. The position of the pulse-height thresholds were determined using a set of ^{137}Cs, ^{22}Na and ^{207}Bi photon sources. The detection efficiencies were calculated using the NEFF7 code [2]. TOF spectra measured with the LG and HG pulse-height branches were matched at neutron energies around 2.5 MeV after correction for the energy dependence of the detection efficiency. The low-energy cut-off of the TOF measurements was at a neutron energy of 500 keV. Measurements with a shadow cone were carried out to subtract neutrons scattered into the detector from the walls and other surrounding structures. More details on the measurement technique are described in [3].

The TOF measurements were compared with TOF spectra calculated with the TARGET code using the nominal target parameters. These TOF spectra were folded with the time structure of the accelerator beam pulse (FWHM ranging from 5.5 ns at E_d = 635 keV to 3.3 ns at E_d = 2664 keV) and the time response of the scintillation detector as calculated with NRESP7 [2]. The time structure of the deuteron pulse was inferred from the shape of the prompt photon peak observed in the TOF spectra.

The tritium used for manufacturing Ti(T) targets is always contaminated with 1 % - 2 % deuterium. This is why neutrons from the D(d,n) reaction are present in neutron fields produced with the T(d,n) reactions and deuteron energies above about 300 keV. Therefore TOF spectra were calculated for targets where the tritium was replaced by the same amount of deuterium. When compared to the experimental TOF spectra, the spectra calculated for Ti(T) and Ti(D) targets were normalised to the respective TOF peaks of the monoenergetic neutrons from the T(d,n) and D(d,n) reactions. The results obtained for the 15.5 MeV, 16 MeV, 17 MeV and 19 MeV fields are shown in Fig. 2a-d. For the 19 MeV measurement, a blank Ti was available which was be used to subtract part of the background neutrons. Therefore Fig. 2d shows the spectral fluence of the 19 MeV field after subtraction of the blank target measurement.

Fig. 2 clearly shows that none of the fields used for the present comparison are free of low-energy background neutrons. In all cases the low-energy continua of collided neutrons as calculated with TARGET are lower than the experimental spectra. The additional contributions can arise from $^{46\text{-}50}$Ti(d,n), ^{107,109}Ag(d,n), ^{16}O(d,n) and ^{12}C(d,n) reactions. Table 2 shows the *Q*-values and threshold energies E_{thr} for these reactions.

For the 19 MeV field, the blank Ti targets obviously compensates only part of the continuum fluence because the blank target is not fully equivalent to the Ti(T) target. As illustrated in Fig. 3, a special problem exists for the experimental 17 MeV spectrum. The deviation of the experimental and calculated spectrum on the left side of the TOF peak is an indication for Ti diffusion into the Ag backing. This conclusion is supported by an analysis of the pulse height spectra produced for small TOF windows on the deviating part of the tail and around the maximum of the TOF peak. These pulse height spectra show that the mean neutron energy in the tail window is around 15 MeV which is consistent with the interpretation given above. The excess neutron fluence in the energy region from 14.2 MeV to 16 MeV resulting from reactions with T nuclei diffused into the Ag backing amounts to 4.3 % of the neutron fluence above 16 MeV. The minimum energy of the uncollided monoenergetic neutrons from the Ti(T) layer is 16.8 MeV.

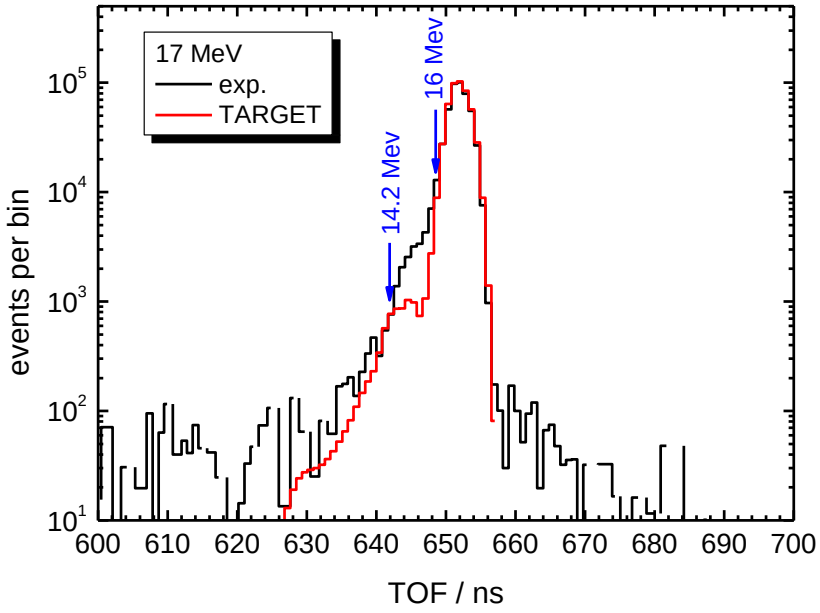

Fig. 3 Indications for diffusion of T into the Ag backing are visible on the left side of the 17 MeV TOF peak in the TOF region corresponding to neutron energies from 14.2 MeV to 16 MeV. The minimum energy of the uncollided monoenergetic neutrons from the Ti(T) layer is 16.8 MeV.

Table 2 *Q*-values and threshold energies E_{thr} for (d,n) reactions producing background neutrons

	Q / MeV	E_{thr} / MeV
^{12}C(d,n)	-0.2817	0.3290
^{16}O(d,n)	-1.6245	1.9291
^{46}Ti(d,n)	2.9410	
^{47}Ti(d,n)	4.6050	
^{48}Ti(d,n)	4.5308	
^{49}Ti(d,n)	5.7261	
^{50}Ti(d,n)	5.7140	
^{107}Ag(d,n)	5.9097	
^{109}Ag(d,n)	6.6910	

In Table 3 the maximum energy produced by ^{48}Ti(d,n) and ^{109}Ag(d,n) for the four neutron fields (the energy loss in the Ti(T) layer was subtracted for the latter reaction) is shown together with the ratio the total neutron fluence Φ_{cont} below the energy E_{cont} and the fluence of ‘monoenergetic‘ neutrons Φ_{peak} above E_{cont} as measured and calculated with TARGET.

Table 3 Maximum neutron energy resulting from ^{48}Ti(d,n)^{49}V and ^{109}Ag(d,n)^{110}Cd and the fluence Φ_{cont} below E_{cont} relative to the peak fluence Φ_{peak} above that energy. The fluence of D(d,n) neutrons was included in the value calculated using the TARGET code.
[1)] after subtraction of the blank target measurement.

E_d / keV	E_{max} / MeV ^{48}Ti(d,n)	E_{max} / MeV ^{109}Ag(d,n)	E_{cont} / MeV	Φ_{cont}/Φ_{peak} exp.	Φ_{cont}/Φ_{peak} TARGET
621	5.124	7.289	11.73	0.039	0.013
778	5.286	7.449	13.05	0.054	0.019
1259	5.776	7.936	12.36	0.065	0.025
2664	7.192	9.250	15.76	0.246[1)]	0.056

The mean energy $\overline{E}_{mon}$ of the spectral fluence of monoenergetic T(d,n) neutrons was determined by fitting the calculated peak corresponding to uncollided neutrons to the peak in the experimental TOF spectrum. From the compression factor and the mean energy of the calculated spectral fluence of uncollided neutrons, the experimental mean energy of the monoenergetic neutrons was calculated. The results are shown in Table 4. The uncertainties of the experimental mean energies were calculated from the uncertainty of the fitting procedure, the flight distance, the TOF calibration and the differential non-linearity of the TOF measurement.

Table 4 Mean energy $\overline{E}_{mon}$ of the monoenergetic neutrons determined experimentally and calculated using TARGET. In addition, the width (FWHM) ΔE_{mon} of the uncollided spectral fluence as calculated with TARGET for the nominal target properties is shown.

E_d / keV	$\overline{E}_{mon}$ / MeV exp.	$\overline{E}_{mon}$ / MeV TARGET	ΔE_{mon} / MeV TARGET	E_{low} / MeV
621	15.51 ± 0.06	15.596	0.620	6.40
778	15.95 ± 0.06	16.020	0.458	6.40
1259	17.05 ± 0.07	17.005	0.238	7.72
2664	18.81 ± 0.10	18.979	0.241	9.08

The mean energy $\overline{E}_{mon}$ and the width ΔE_{mon} of the spectral distribution of uncollided neutrons as calculated with TARGET should be used for the analysis of the fluence measurements. To arrive at spectral fluence distributions which can by used by the participants to correct their measurement for the contributions of low-energy neutrons, the following procedure was adopted:

The normalisation factors determined from the comparison of experimental and calculated TOF spectra as shown in Fig. 2 were applied to the TOF spectra calculated with TARGET prior to the additional TOF broadening caused by the finite duration of the beam pulses and the time response of the scintillation detector. After that, experimental and calculated TOF spectra were transformed from TOF scale to energy scale. 'Synthetical' spectral fluences were produced by joining the TARGET spectra and the experimental spectra at the energies E_{low} indicated in Table 4. In this way, spectral fluences were obtained which have the increased low-energy continua as experimentally determined and high-energy peak regions which are not distorted by the broadening caused by the time resolution of the TOF measurements. These spectral fluences are available in numerical form together with the spectral fluences calculated with TARGET for the nominal target properties. Fig. 4a-d shows a comparison of experimental and calculated spectra. The energy E_{low} is indicated by the arrows.

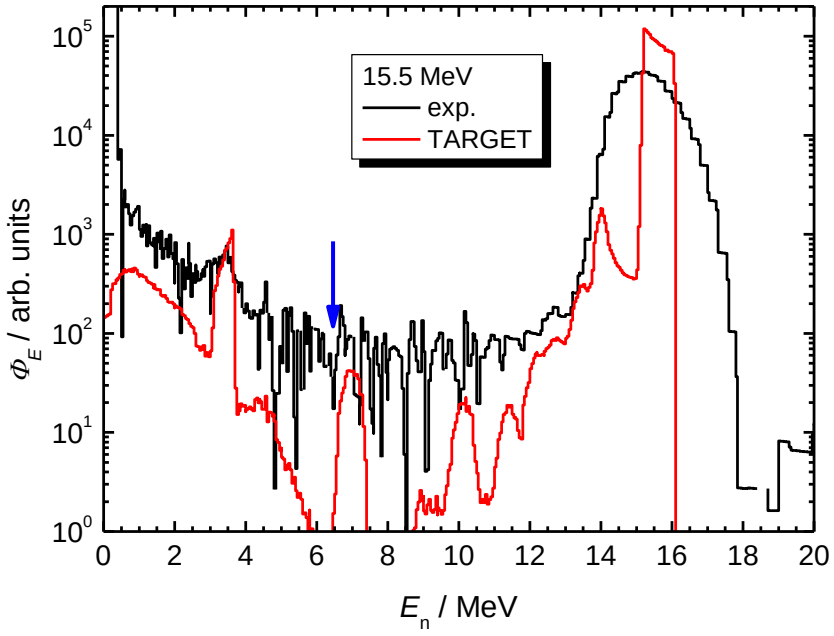

Fig. 4a Measured (black histogram) and calculated (red solid line) spectral fluence for E_d = 621 keV. The arrow shows the energy E_{low} where the experimental spectrum for $E < E_{low}$ was joined to the calculated spectral fluence for the peak region $E > E_{low}$.

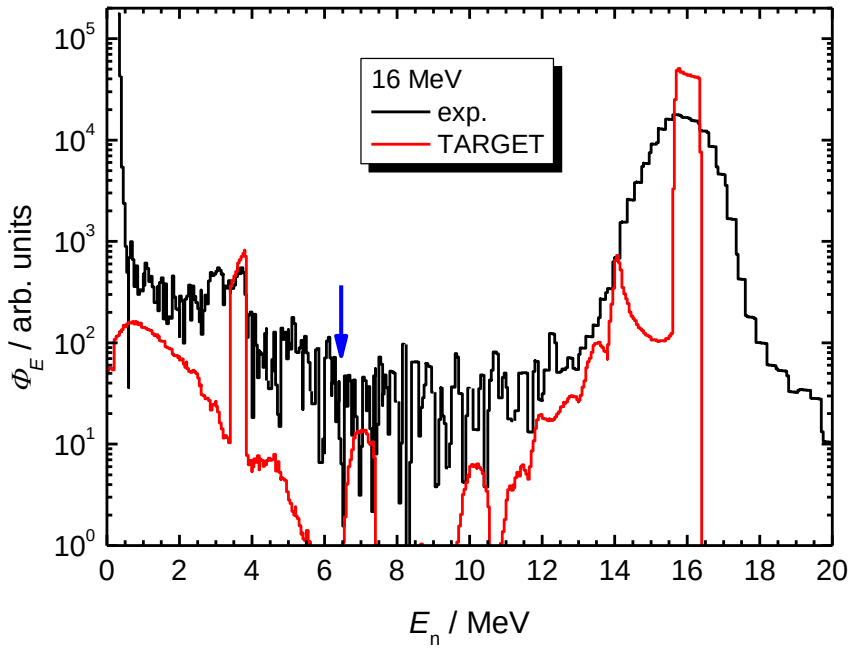

Fig. 4b Measured (black histogram) and calculated (red solid line) spectral fluence for E_d = 778 keV.

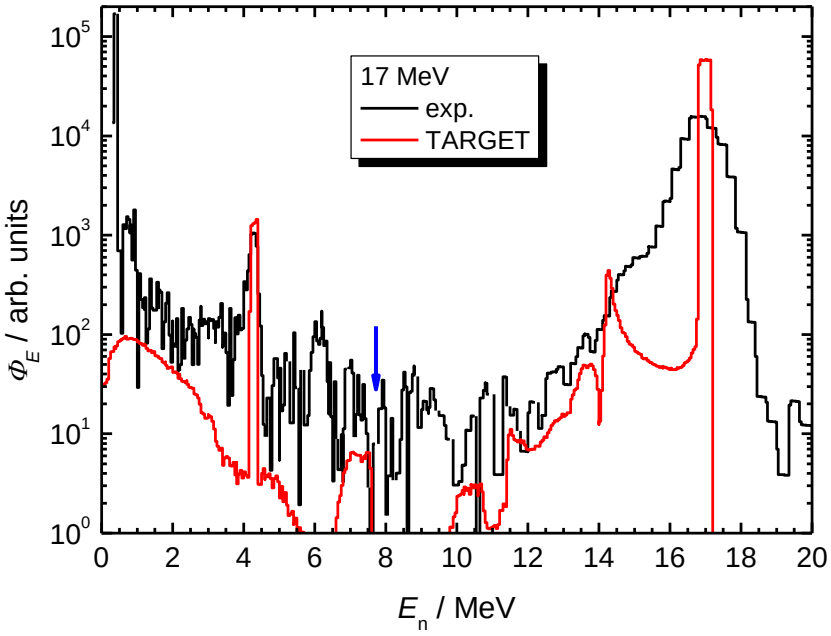

Fig. 4c Measured (black histogram) and calculated (red solid line) spectral fluence for E_d = 1259 keV.

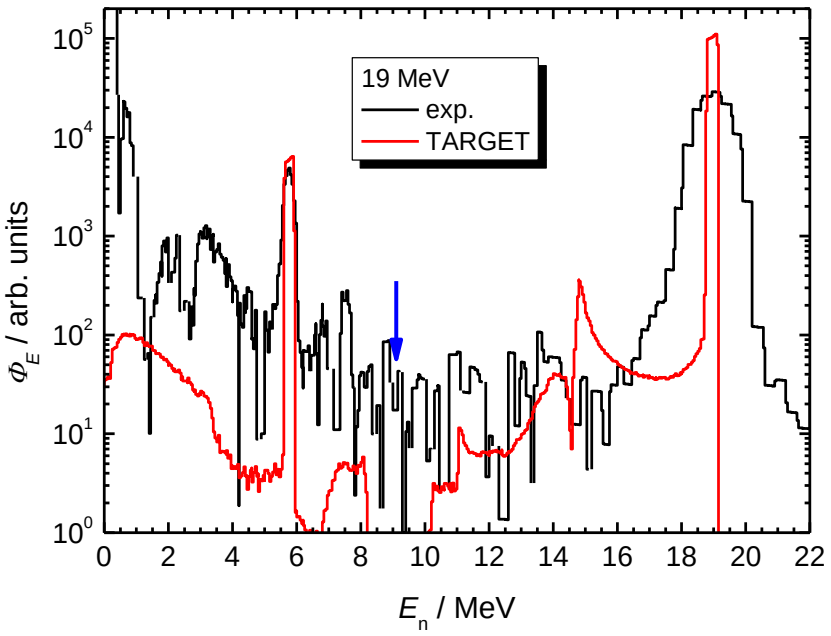

Fig. 4d Measured (black histogram) and calculated (red solid line) spectral fluence for E_d = 2664 keV. The blank target measurement was subtracted from the experimental spectral fluence.

References for Appendix 2

[1] D. Schegel, *TARGET user's manual*, PTB laboratory report PTB-6.42-05-2, Physikalisch-Technische Bundesanstalt Braunschweig 2005

[2] G. Dietze, H. Klein, *NRESP4 and NEFF4*, PTB report PTB-ND-22, Physikalisch-Technische Bundesanstalt Braunschweig 1982, with an informal supplement describing the changes in version 7, 1991

[3] R. Böttger, S. Guldbakke, H. Klein, H. Schölermann, H. Schuhmacher and H. Strzelczyk, *Problems associated with the production of monoenergetic neutrons*, Nucl. Instr. and Methods A282 (1989), 358 - 367

Appendix 3:

EUROMET Project 822 'Comparison of Neutron Fluence Measurements for Neutron Energies of 15.5 MeV, 16 MeV, 17 MeV and 19 MeV'

Determination of the monitor readings

Introduction

At the PTB low-scatter facility, two precision long counters mounted at neutron emission angles of 16° and 100°, and a ^{3}He proportional counter inside a cover made from borated polyethylene are used as neutron-sensitive monitors. In addition, the beam charge is measured and a Geiger Müller counter is available for monitoring the production of photons. These monitors are used to relate the fluence measurements with the different reference instruments participating in the comparison exercise. These monitors reading have to be corrected for dead time loss and for inscattering from reference instruments in the neutron field.

Calculation of the correction factors

The dead time of the monitors are defined by fixed artificial dead times τ introduced by special dead time modules behind the discriminators. The dead time correction is given by $k_{\mathrm{dt}} = 1/(1-\tau\cdot(\mathrm{d}N/\mathrm{d}t))$.

The correction for inscattering is carried out by performing measurements without reference instruments in the neutron field (free-field measurement) immediately before or after a measurement with the reference instruments. The correction factor k_{sc} for inscattering can be calculated from such a pair of measurements on the assumption that the beam charge Q is a 'good' monitor for a short time interval:

$$k_{\mathrm{sc}} = \left(\frac{k_{\mathrm{dt}}N}{Q}\right)_{\substack{(\mathrm{free}\\ \mathrm{field})}} \cdot \left(\frac{Q}{k_{\mathrm{dt}}N}\right)_{\substack{(\mathrm{ref.}\\ \mathrm{instr.})}}$$

For the measurements with the PTB recoil proton telescope (RPT), the correction factors k_{sc} were usually calculated form the free-field measurement and the background measurement with the radiator rotated by 180°. With the IRMM RPT, measurements were carried out at different distances. Therefore individual correction factors had to be calculated for each distance. Since only one free-field measurement was performed after the measurements with the IRMM RPT, some of the correction factors were calculated from pairs of measurements which were not adjacent in time. For the NPL long counter (LC), a measurement without and with shadow cone and a free-field measurement were performed at several distances. Here it had to be assumed that the beam charge Q was a good monitor over the time required for the LC and free-field measurements at each distance.

Fig. 1a-e shows the ratio of the corrected readings $N_{\mathrm{cor}} = k_{\mathrm{dt}}\cdot k_{\mathrm{sc}}\cdot N$ of the two long counter monitors at 16° (NM) and 100° (PLC) to the beam charge Q. Generally, these ratios are stable within less than ±1 %. The ratios for each detector were normalised to their mean values for the respective energy. Only for the measurements with the PTB RPT at 15.5 MeV and 19 MeV, somewhat larger deviations are observed. The PTB RPT was always the first instrument in the morning. Therefore these drifts can be attributed to warming-up effects of the accelerator and the beam transport system which influence the beam current measurement. The attached EXCEL spreadsheets give the corrected readings N_{cor} for each measurement and an overall uncertainty estimated from the variance of the (N_{cor}/Q) ratios. It is suggested that all

participants use the $N_{\mathrm{cor}}^{(\mathrm{NM})}$ value for the 16° monitor (NM) to normalize their measurements and calculate the monitor calibration factor $C = N_{\mathrm{cor}}^{(\mathrm{NM})} / \Phi$.

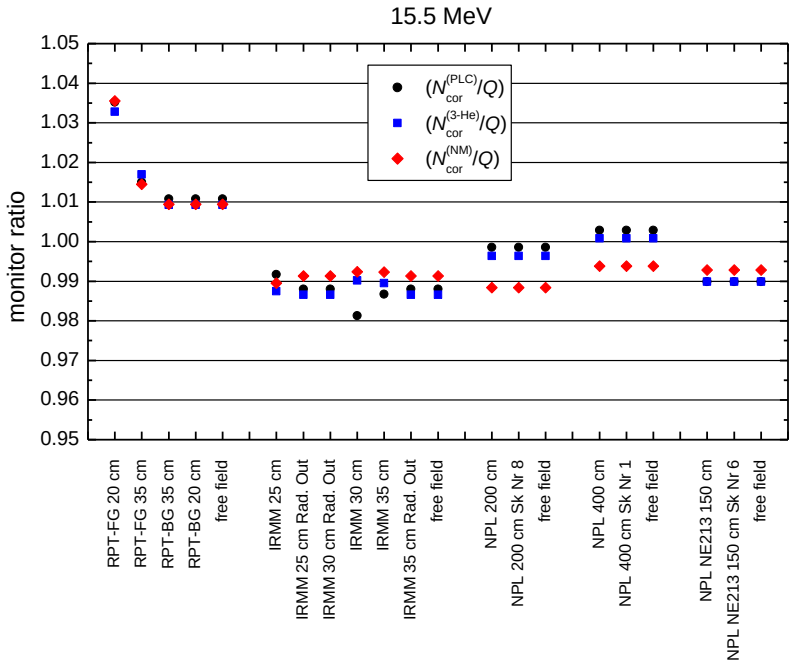

Fig. 1a Ratio of the corrected monitor counts N_{cor} to the beam charge Q for the 15.5 MeV measurement on 2004-12-09.

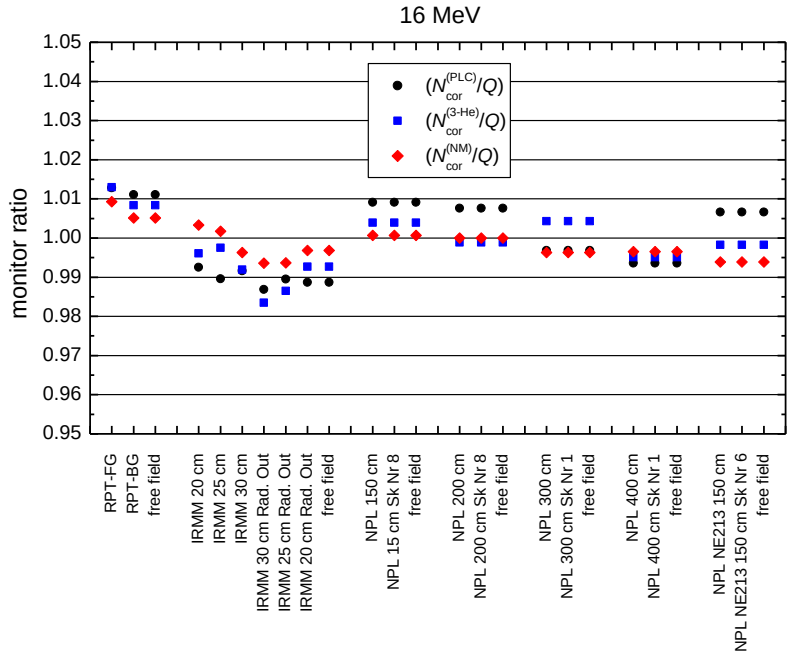

Fig. 1b Ratio of the corrected monitor counts N_{cor} to the beam charge Q for the 16 MeV measurement on 2004-12-06.

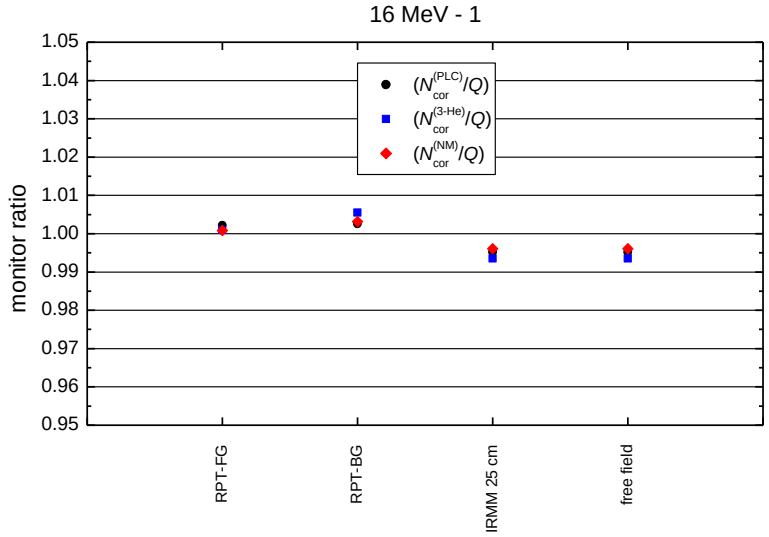

Fig. 1c Ratio of the corrected monitor counts N_{cor} to the beam charge Q for the 16 MeV measurement on 2004-12-10.

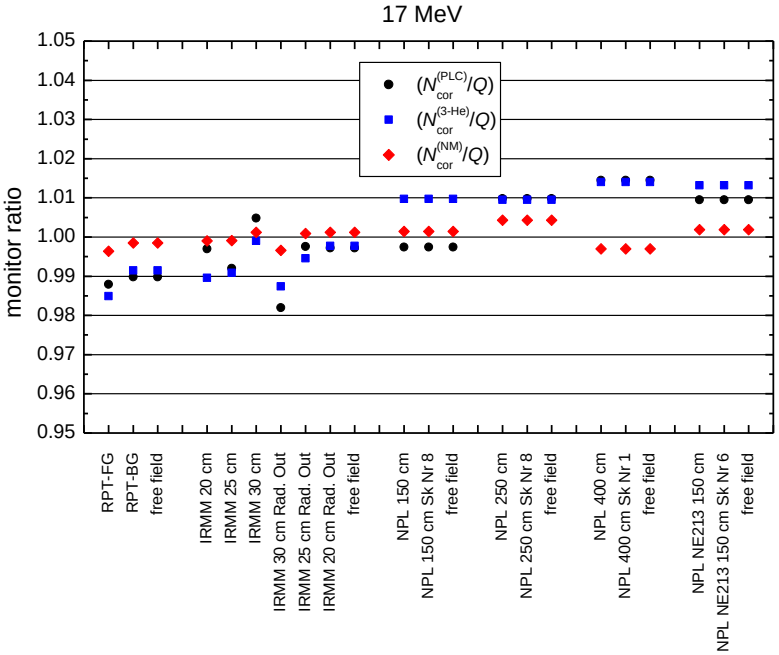

Fig. 1d Ratio of the corrected monitor counts N_{cor} to the beam charge Q for the 17 MeV measurement on 2004-12-07.

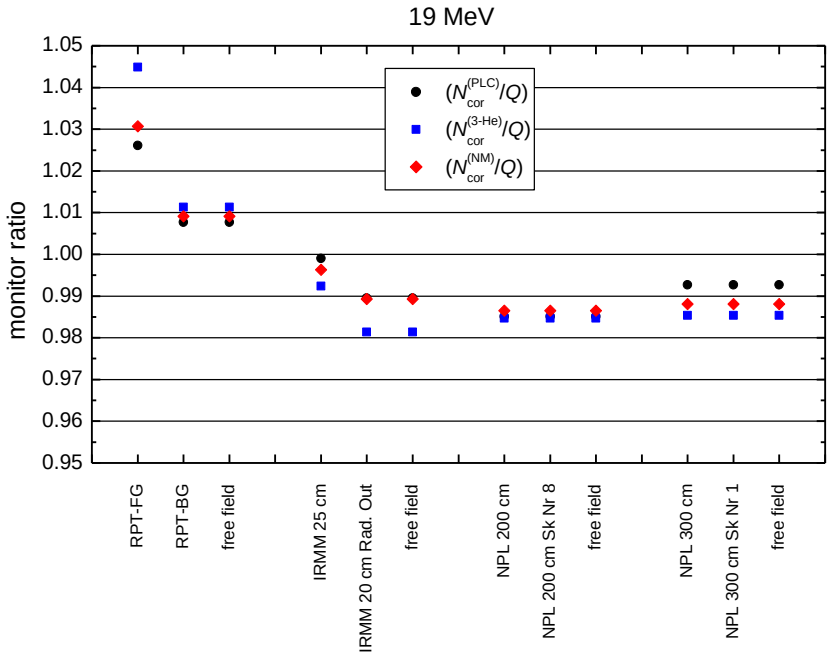

Fig. 1e Ratio of the corrected monitor counts N_{cor} to the beam charge Q for the 19 MeV measurement on 2004-12-08.

Monitor readings for the Al activation measurement

A measurement with the PTB RPT was carried out before the start of the Al activation. The inscatter correction for this measurement was extrapolated from measurements at 15.5 MeV and 16 MeV. Correction factors k_{sc} of 0.992 ± 0.008 and 0.988 ± 0.004 were obtained for the PLC and NM monitors, respectively. Fig. 2 shows the ratio of the corrected monitors counts N_{cor} to the beam charge Q.

The activation was started at 2005-04-20, 10:25:00 (MEST) and stopped at 23:00:00 (MEST). The monitor readings were recorded in time intervals of 600 s. During the RPT measurement, a decrease of the ratios is observed followed by a slight drift for most of the activation run and a step-like change close to the end of the activation. Since the ratio of the two neutron monitors is very constant, the drifts must be due to changes in the beam charge measurement. Therefore the NM monitor should be used for the analysis of the Al activation measurement.

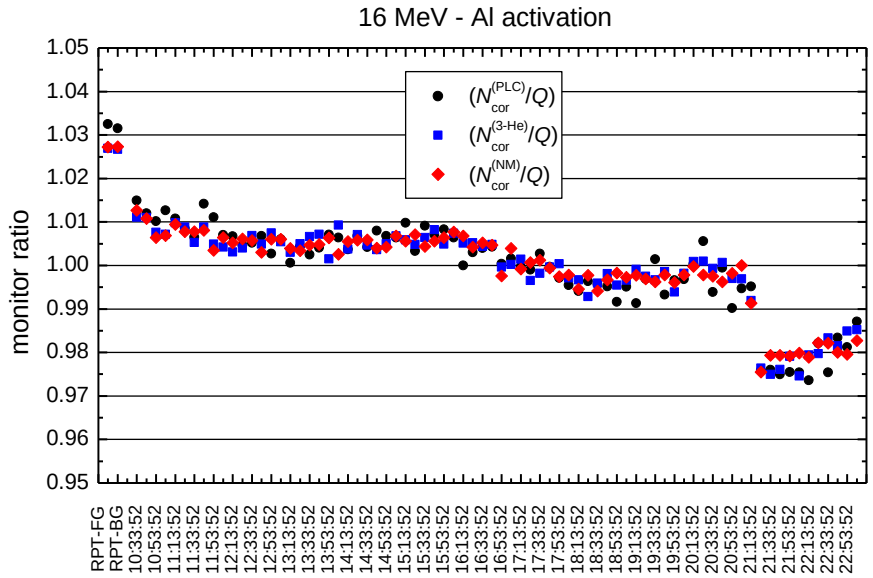

Fig. 2 Ratio of the corrected monitor counts N_{cor} to the beam charge Q for the 16 MeV Al foil activation measurement on 2005-04-20.